ChemPubSoc Europe

DOI: 10.1002/ejic.201601230

EurJIC European Journal of Inorganic Chemistry

Full Paper

Mechanochromic Luminescence

Lead(II) 4,4′-Bipyridine *N*-Oxide Coordination Polymers – Highly Phosphorescent Materials with Mechanochromic Luminescence Properties

Oksana Toma,[a] Nicolas Mercier*[a] Magali Allain,[a] Francesco Meinardi,[b] and Chiara Botta*[c]

Abstract: In the $Pb^{II}X_2$/bp4mo (4,4′-bipyridine *N*-oxide) system, four coordination polymers (CPs) with the formulation of $[PbX_2(bp4mo)]$ are obtained. Compounds **1** and **2**, in which X = Cl and Br, are polymorphs whose acentric structures are based on 2D CPs. On the contrary, the compound **3** (X = I) shows a close, but centrosymmetrical, structure compared with the ones of **1** and **2**. Finally, the structure of compound **4**, in which X = NO_3^-, is described by two-interpenetrated 3D networks. They all exhibit phosphorescence properties characterized by a broad emission band at around 600 nm, with lifetimes longer than tens of μs and quite high quantum yields that increase in the halide series from 6 % (**1**) to 27 % (**3**) and up to 34 % for **4**. They also exhibit mechanochromic luminescence (MCL) properties: the grinding (g) of samples **1**–**4** involves nearly complete extinction of the luminescence, as well as a crystal to amorphous transition of the corresponding samples **1-g** to **4-g**. This phenomenon, which can be also considered a crystallization-enhanced emission process, is reversible either by heating, exposure to vapour (H_2O, acetone) or by recrystallization in a few drops of acetone; however, it is accompanied by a loss of emission intensity. These compounds represent the first examples of MCL materials based on Pb^{2+}.

Introduction

In the field of metal complexes and coordination polymers (CPs), the search for highly luminescent solid-state materials and materials with tuneable luminescence is of great interest due to their potential applications in lighting and displays, memory devices and sensors.[1–4] In this context, we recently discovered a new family of luminescent metal complexes based on two bipyridine *N*-oxide ligands: 4,4′-bipyridine *N*-oxide (bp4mo) and 2,2′-bipyridine *N*-oxide (bp2mo). These ligands, which are not commercially available, have been rarely used in the field of coordination chemistry, in contrast with the well-known symmetrical 4,4′-bipyridine or 4,4′-bipyridine *N*,*N*′-dioxide.[5] Up to now, only a series of four metal complexes based on 4,4′-bipyridine *N*-oxide were reported by Loeb et al.[6] and, in 2012, we described the first coordination polymer based on bp4mo ligands $[PbCl_2(bp4mo)]$, which is characterized by a bright emission in the orange-red region.[7] Focusing on Bi^{3+} metal ions, luminescent complexes based on bipyridinium derivatives ligands including a pyridyl *N*-oxide group (*N*-alkyl-4,4′-bipyridinium *N*′-oxide) were first obtained,[8] but the most interesting and promising results were obtained in the Bi^{3+}/bp2mo and Bi^{3+}/bp4mo systems where three polymorphic complexes, $[BiBr_3(bp2mo)]$[9,10] and two highly luminescent compounds $(TBA)[BiBr_4(bp4mo)]$ and $[BiBr_3(bp4mo)_2]$,[11] were characterized (TBA = tetrabutylammonium). A complete study of their luminescence properties, also supported by DFT calculations, has demonstrated that they possess aggregation-induced phosphorescence (AIP). AIP materials are especially interesting because they often exhibit mechanochromic luminescence (MCL).[12–14] MCL implies tuneable luminescence properties, either a change of emission intensity or a change of emission wavelength, when mechanical forces are applied.[2–4] When a change of emission intensity occurs due to the degree of the crystallinity, the process can be also considered as a crystallization-enhanced emission process. Such materials can find applications in different fields, such as luminescence switches, mechanosensors, data storage or security papers. Two main categories of MCL materials are known, pure organic materials[15,16] and metal complex materials.[4,17–20] Typically, grinding of a pristine crystallized powder involves the amorphization of the sample, together with a redshift and/or quenching of the emission. Both phenomena, loss of crystallinity and emission change, are explained by modifications of weak interactions, such as π–π, van der Waals or H bonding, in the molecular structures upon grinding. These interactions mainly involve organic moieties, which explains why the majority of MCL materials are organic com-

[a] *MOLTECH ANJOU, UMR-CNRS 6200, Université d'Angers, 2 Bd Lavoisier, 49045 Angers, France*
E-mail: nicolas.mercier@univ-angers.fr
http://moltech-anjou.univ-angers.fr/Joomla/index.php/fr/component/content/article/9-uncategorised/89
[b] *Dipartimento di Scienza dei Materiali, Università degli Studi di Milano Bicocca, Via Cozzi 55, 20125 Milano, Italy*
[c] *Istituto per lo Studio delle Macromolecole (ISMAC) CNR, Via Corti 12, 20133 Milano, Italy*
E-mail: c.botta@ismac.cnr.it

Supporting information and ORCID(s) from the author(s) for this article are available on the WWW under http://dx.doi.org/10.1002/ejic.201601230.

pounds and most of the MCL metal complexes are based on the noble metals of Pt^{II}[17] and Ir^{III}[18] for which luminescence properties are very sensitive to the type of ligands due to the LMCT nature of the emission. The reversibility of the process, which consists of a recrystallization of the metastable ground sample, together with the recovery of the initial emission, can typically be achieved by heating, exposure to vapours of water or organic solvents, or by fast recrystallization when a few drops of solvent are deposited on the sample.

Reversible MCL properties have been found for most of the bipyridine complexes, including the α- and γ-$[BiBr_3(bp2mo)_2]$[10] and the (TBA)$[BiBr_4(bp4mo)]$,[11] which were the first bismuth-based MCL materials. While Bi^{3+} and bp4mo provide highly luminescent materials with MCL properties, an obvious question is: do complexes based on Pb^{2+} and bp4mo exhibit such properties, too?

Here we report on four Pb^{2+}-bp4mo metal complexes. Besides the known $[PbCl_2(bp4mo)]$ compound (**1**), we describe the synthesis and crystal structures of three other compounds with the formulation of $[PbX_2(bp4mo)]$, X = Br (**2**), X = I (**3**) and X = NO_3 (**4**). We show that the Cl and Br compounds, which are 2D CPs, are isostructural (acentric space group), while the I compound crystallizes in a close, but centrosymmetrical, structure. When X = NO_3, a 3D CP is defined and the whole structure results from the interpenetration of two of such networks. The optical characterization of **1**–**4** shows that all materials exhibit quite large phosphorescence quantum yields (QYs), which increase from 6 % to 28 % in the Cl to I series (**1** to **3**) and up to 34 % for the NO_3 compound (**4**). Finally, the MCL properties, including the reversibility of the process, are reported, showing that all compounds exhibit nearly complete extinction of the luminescence upon grinding.

Results and Discussion

Description of the Crystal Structures

All compounds **1**–**4** were obtained as nice crystals from a slow liquid–gas diffusion synthesis. The crystal structure of **2** is isomorphous to that of **1**, which was already described.[7] It consists of 2D coordination polymers (CPs) built from the coordination of metal ions by bp4mo molecules along one direction and by edge sharing of lead octahedra in the perpendicular direction (Figure 1). Two kinds of Pb^{2+} polyhedra are counted: those bound to two oxygen atoms of the pyridyl *N*-oxide part of bp4mo $[Pb(1)O_2Br_4]$ and those bound to two nitrogen atoms of the pyridyl parts of bp4mo $[Pb(2)N_2Br_4]$. The presence of these two types of polyhedra, as well as the zig-zag type coordination, precludes any symmetry centre in this 2D CP. The overall structure, which results from the stacks of these 2D CPs held together by weak H···Br interactions[21] (Figure S1), remains acentric. The crystal structure of **3** is very similar to that of **1** or **2**: there are two kinds of lead polyhedra, $Pb(1)O_2I_4$ and $Pb(2)N_2I_4$, and the same type of 2D coordination polymer is found with inorganic chains of edge-sharing octahedra along one direction and the coordination of Pb^{2+} through bp4mo molecules along the perpendicular direction (Figure 1). However, **3** differs from the previous structure, mainly due to the presence of a centre of symmetry located on Pb(1) as a result of a peculiar arrangement of the two bp4mo molecules bound to Pb(1). Finally, we notice that the zig-zag type coordination is also observed in the structure of **3**, but with a periodicity which is twice the periodicity found in the structures of **1** and **2**. Even if the lead environment can be considered as nearly octahedral, the bond lengths and bond angles deviate from ideal values. This results from the presence of two types of atoms, as well as of distortions. As regards the $Pb(2)N_2X_4$ polyhedra, the Pb–N bond lengths are similar [**2**: 2 × 2.643(16) Å; **3**: 2 × 2.658(13) Å], while the N–Pb–N bond angles deviate from 180° [**2**: 162.8(3)°; **3**: 171(3)°Å] and the Pb–X bond lengths are asymmetrical (two short and two long, with the short bonds being opposite to the long ones) [**2**: 2 × 2.916(2) Å and 2 × 3.133(2) Å; **3**: 2 × 3.145(1) Å and 2 × 3.294(1) Å], which usually reveals the stereoactivity of the Pb^{2+} ns^2 lone pair (Figure 2). As regards the $Pb(2)O_2X_4$ polyhedra, the Pb–O bond lengths are similar in both structures [**2**: 2 × 2.531(13) Å; **3**: 2 × 2.530(10) Å]. Two Pb–X bond lengths are also present in **2** and **3**, but in this case, they are quite close [**2**: 2 × 2.990(2) Å and 2 × 3.049(2) Å; **3**: 2 × 3.174(1) Å and 2 × 3.228(1) Å]. We note that because of the symmetrical configuration of Pb(1) in **3**, the two short bonds, as well as the two long bonds, are in opposite directions, in contrast with the situation described for PbN_2X_4 and for PbO_2Br_4. The overall structure results from the stacks of the 2D CPs held together by weak H···I interactions (Figure S2).

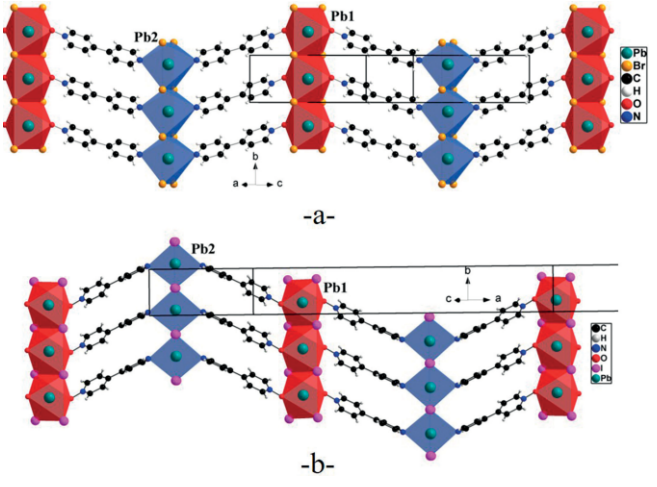

Figure 1. The 2D coordination polymer in $[PbX_2(bp4mo)]$, X = Br (**2**) (a) and X = I (**3**) (b) showing the two kinds of octahedra, PbN_2X_4 (blue) and PbO_2X_4 (red), as well as the acentric (X = Br) and centric (X = I, symmetry centre on Pb1 atoms) nature of the networks.

The compound **4** crystallizes in the *Pbca* centric space group, with the asymmetric unit including only one independent Pb^{2+} ion surrounded by three bp4mo molecules and four nitrate anions (Figure 2c). Molecules of bp4mo are coordinated to Pb^{2+} through the oxygen atom of the pyridyl *N*-oxide part for two of the three and through the nitrogen atom for the third one. The nitrate ions are linked to the metal ion either by two of their oxygen atoms for two of the four or by only one for the two others. The oxygen atoms belonging to the bp4mo molecules and some of the oxygen atoms of the nitrates are shared

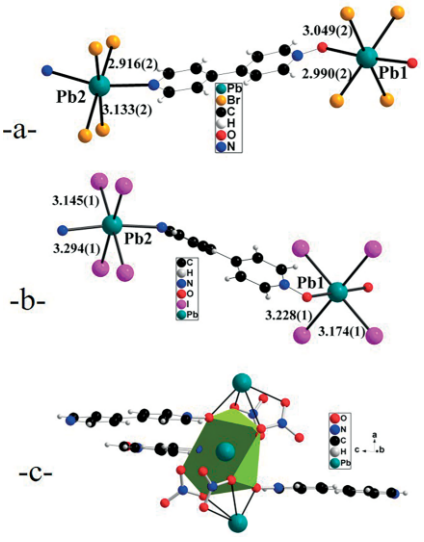

Figure 2. Environment of Pb^{2+} ions in the structures of **2** (a, PbN_2Br_4 and PbO_2Br_4), **3** (b, PbN_2I_4 and PbO_2I_4) and **4** (c, Pb^{2+}linked to 3 bp4mo molecules and 4 NO_3^- anions), as well as selected Pb–X (X = Br, I) bond lengths.

by two Pb^{2+} ions (Figure 2), leading to inorganic chains of face-sharing lead polyhedra running along the *a* axis (Figure 3). The connection of chains via the bp4mo molecules defines an open 3D coordination polymer with square-like channels. The overall structure results from the interpenetration of two of such 3D networks, precluding any porosity (Figure 3). As a consequence, a stack of bp4mo molecules occurs along the *a* axis, but it is worth noting that two adjacent molecules are perpendicular to each other and that the shortest intermolecular contact is the 3.84 Å between the two carbon atoms belonging to the central C–C bonds. In the structure of **1**–**3**, the face-to-face stacking of bp4mo molecules is more efficient, as indicated by the short distances between carbon atoms of 3.53 Å (**2**), 3.50 Å (**3**) and 3.58 Å (**1**). Such different pi-stacking situations observed in **1**–**4** have been already described in the literature.[22]

Luminescence and MCL Properties

All the four Pb^{2+}-bp4mo metal complexes display a strong luminescence in the solid state, while their properties in solution cannot be determined due to their low solubility. Their emission efficiencies are much higher in the crystal than in the amorphous phase (see MCL properties). This is similar to the previously reported Bi^{3+}/bp4mo- or bp2mo-based complexes,[9,11] for which AIP properties have been demonstrated. In Figure 4, the absorption and emission spectra are reported for the four compounds. The absorption spectra, obtained on powders dispersed in KBr pellets, display a broad low-energy band at about 350–375 nm (**1**, **2**: 360 nm, **3**: 375 nm, **4**: 350 nm) and a sharp high-energy peak at 300–305 nm. In analogy with the Bi^{3+}-based compounds, the low-energy band can be assigned to a metal (inorganic part) to ligand (bp4mo) charge transfer (CT) transition, while the high-energy one has intraligand CT character.[11]

The photoluminescence spectra of the four compounds are very similar. They are dominated by a vibronic progression originating at about 600 nm, with a separation between the vibrational replicas of about 150 meV. Its lifetime is in the range of tens of µs and more (**1**, **2**: 250 µs, **3**: 40 µs, **4**: 1.5 µs and 700 µs, Figure 5), a clear indication of a partially forbidden transition which gives rise to a phosphorescent emission. A second weak emission around 550 nm is also present with the relative intensity dependent on the sample. It shows a different lifetime with respect to the main peak (a few µs instead of tens or hundreds of µs – see inset of Figure 5 for **4**), which implies that it originates from a different electronic transition, tentatively ascribed to structural defects.

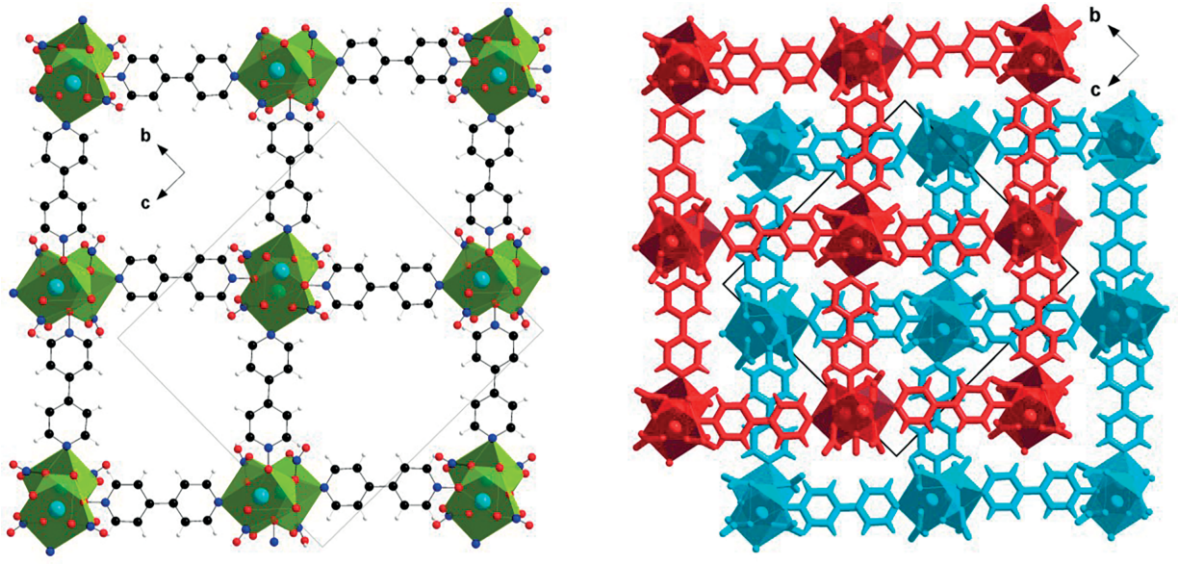

Figure 3. The structure of $[Pb(NO_3)_2(bp4mo)]$: the 3D open framework showing square channels along the *a* axis (left); and general view along *a* showing the interpenetration of two 3D coordination polymers (right).

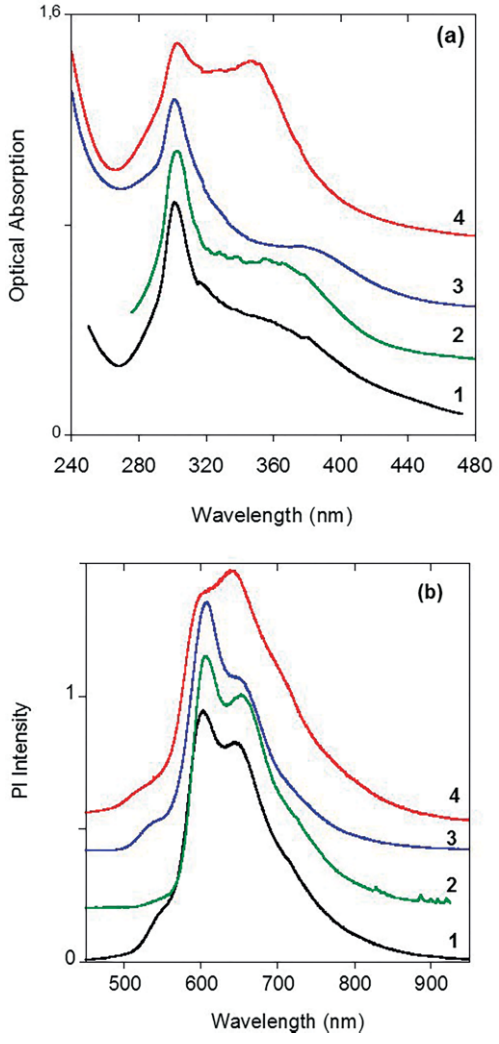

Figure 4. (a) Optical absorption of the structures dispersed in KBr pellets; (b) photoluminescence spectra of the crystals excited at 380 nm. The spectra are vertically shifted for clarity.

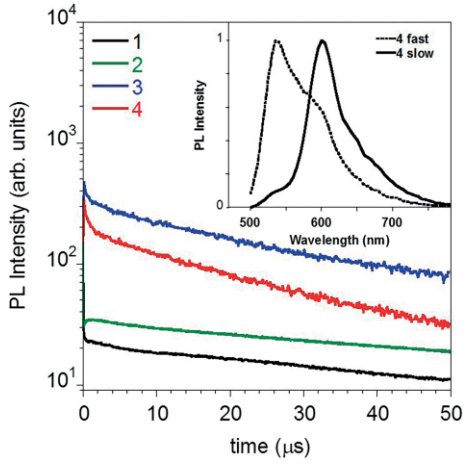

Figure 5. Photoluminescence (PL) time decay of structures **1**–**4** measured at 600 nm. Inset: PL spectra of structure **4** integrated in the 0–1 μs (fast) and in the 5–20 μs (slow) time delay window.

The quantum efficiencies of the red phosphorescence are 6 %, 22 %, 27 % and 34 % for **1**, **2**, **3** and **4**, respectively. We notice that in the isostructural series **1**–**3**, the quantum efficiency increases along with the halide's weight, from 6 % (Cl) to 27 % (I). This is probably due to a heavy atom effect which favours the intersystem crossing (ISC). This hypothesis is also confirmed by a lack of any clear correlation between the observed quantum efficiencies and emission lifetimes, suggesting that the phosphorescence intensity is mainly determined by the number of the generated triplet states upon excitation, i.e., by the ISC efficiency, and not by changes in the lifetimes of these states.

Upon grinding each of the four samples in a mortar for a few minutes, the position of their emission band does not show relevant changes (only a variation of the relative intensity of the different peaks is observed – see Figure S3), but its intensity rapidly decreases to nearly complete extinction. This behaviour differs from the one observed in the Bi^{3+}/bp4mo[11] and Bi^{3+}/bp2mo[10] systems, where a redshift of the emission band occurs. Nevertheless, as observed in most of the MCL materials, the grinding of samples **1**–**4** involves an amorphization of the crystalline samples, as revealed by the absence of diffraction lines in the corresponding X-ray powder diffraction (XRPD) of **2-g** and **3-g** (Figures 6b and 7), **1-g** and **4-g** (Figures S4 and S9). The occurrence of changes in the crystal structure induced by the grinding are supported by the differential scanning calorimetry (DSC) analysis that shows, in all the ground samples, the appearance of a new exothermic peak at 55 °C for **2** (Fig-

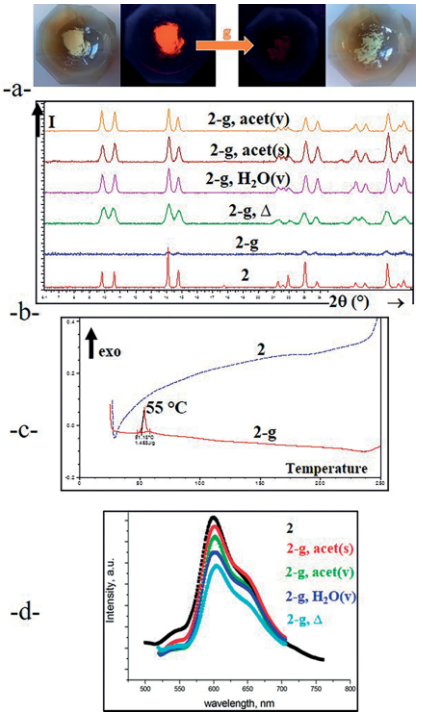

Figure 6. MCL properties of **2**. (a) Photos under ambient light and UV irradiation of the as-synthesized compound (left) and after grinding (**2-g**) (right); (b) XRPD patterns of **2**, **2-g** and **2-g** after heating treatment (**2-g, Δ**), fuming (a few hours) [**2-g, $H_2O_{(v)}$** and **2-g, $acet_{(v)}$**] and fast concentration of an acetone solution [**2-g, $acet_{(s)}$**]; (c) DSC curves of **2** and **2-g**; (d) PL spectra of **2**, **2-g, Δ**, **2-g, $H_2O_{(v)}$**, **2-g, $acet_{(v)}$** and **2-g, $acet_{(s)}$**.

ure 6c), at 50 °C for **1** (Figure S5), at 65 °C for **3** (Figure S7) and at 60 °C for **4** (Figure S10). This exothermic peak is assigned to a recrystallization of the samples, as confirmed by powder diffraction measurements (see Figure 6b, **2-g,** Δ), that clearly show exactly the same XRPD spectra of the as-synthesized compound **2**. The amorphous-to-crystalline reversible process is also observed for the luminescence properties. In particular, the recrystallized compounds exhibit phosphorescence whose shape and position well match the initial compound spectrum [Figure 6d (**2**) and Figures S6, S8 and S11 for **1**, **3** and **4**, respectively].

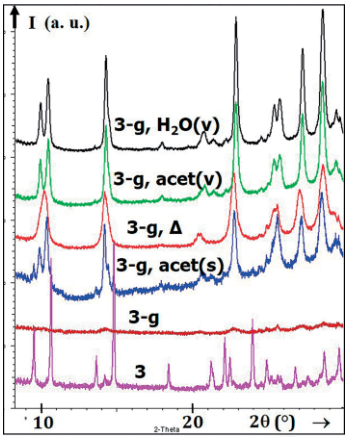

Figure 7. XRPD patterns of the as-synthesized compound (**3**), the ground sample (**3-g**) and the ground sample after heating (**3-g,** Δ), after fuming [**3-g, $H_2O_{(v)}$** and **3-g, $acet_{(v)}$**] and after a few drops of acetone were deposited on the ground sample and evaporated [**3-g, $acet_{(s)}$**].

The reversibility of the amorphous-to-crystalline transition is obtained not only by heating, but also by fuming (exposure of ground samples to a saturated atmosphere of different solvents during a few hours), as shown in Figure 6b for water and acetone vapour exposure. Moreover, the amorphous-to-crystalline transition is obtained also by fast concentration of a few drops of acetone deposited on the ground samples (Figure 6b). The full reversibility of the amorphous-to crystalline process using these different methods (heating, fuming, solution) is also demonstrated for **1-g** and **4-g** (Figures S4 and S9), while a peculiar situation occurs for the iodide compound **3**. In this case, when recrystallization of **3-g** is performed by heating or using a slow process (fuming), a new phase **3′** is obtained. Its diffraction pattern (Figure 7) resembles the XRPDs of the compounds **1** and **2** with, in particular, two close lines around $2\theta = 10°$ (see Figure S12 for a direct comparison). While the crystal structure of **3** is centric, the new **3′** phase, in the hypothesis that it is isostructural to **1** and **2**, should be acentric (see "Description of Crystal Structures" for **1**, **2** and **3**). On the other hand, when a fast recrystallizing process is used (solution deposition), both the two phases, **3** and **3′**, are obtained [Figure 7, **3-g, $acet_{(s)}$**]. These results would suggest that **3′** is the thermodynamic phase, while **3** is a kinetic phase. However, the synthesis of crystals by using the room temperature liquid–gas diffusion method, while a slow process, always leads to compound **3**. Moreover, we have performed XRPD of **3** and **3′** at different temperatures up to 200 °C (thermodiffractometry, see Figures S13 and S14), which shows that there is no transformation of **3′** into **3** or **3** into **3′**. To check the acentric nature of samples **1**, **2**, **3** and **3′**, they were irradiated with a high-power Nd:Yag laser at 1064 nm. The second harmonic (green light, 532 nm) generation was observed for **1**, **2** and **3′**, confirming their acentric nature.

Finally, we must notice for all compounds, that a loss of crystallinity occurs after a grinding/recrystallization cycle. This is clearly shown by the broadening of X-ray diffraction lines in the corresponding XRPD compared with the diffraction lines of the as-synthesized compounds. Moreover, we observe that the broadening of the diffraction lines is greater when recrystallization is obtained by heating the ground samples (see, for instance, Figures 6b and 7 for **2** and **3**, respectively). Another consequence is the loss of emission intensity. Thus, we performed grinding/recrystallization cycles for compound **4** using acetone solution in the recrystallization process. We observed a reduction (about a factor of 0.6) of the emission intensity of the compound after the first two grinding/recrystallization processes, while the following cycle did not show further reduction (Figure S15). This confirms the crystallization-enhanced emission process: lower emission efficiencies for low-crystallinity samples (after heating of the ground samples, for instance) and high emission efficiencies for high-crystallinity samples (as-synthesized compounds or after recrystallization of the ground samples by using a few drops of acetone).

Conclusion

In this work, we show that the coordination compounds [PbX_2(bp4mo)] involving Pb^{2+} metal ions and bp4mo molecules are highly phosphorescent, with quantum yields up to 34 %, for **4** (X = NO_3). In the halide series, the increase of the QY from 6 % for **1** (X = Cl) to 28 % for **3** (X = I) has been ascribed to a corresponding increase of the ISC efficiency within the heavy halide-based materials. These findings demonstrate that the association of bp4mo molecules with ns^2 heavy metal ions belonging to block p, either Bi^{3+}[9–11] or Pb^{2+} (this work), gives rise systematically to materials with strong luminescence in the solid state. All these compounds exhibit reversible MCL properties. In particular, upon grinding, the sample amorphization induces a dramatic decrease of the phosphorescence intensity. This process is reversible, as the recrystallization, obtained by heating, by fuming or by fast evaporation of a few drops of acetone, allows the emission to recover. However, due to a partial loss of crystallinity after the first grinding/recrystallization cycles, a reduction of emission intensity is observed. This is known as a crystallization-enhanced emission process. It is worth noting that the grinding/recrystallization process of **3** leads to stabilizing the derived structure **3′**, which cannot be obtained directly by synthesis or through a solid-state reaction from **3** and which cannot be transformed into **3**. Interestingly, while the grinding induces a shift of the emission band for Bi^{3+}- and bp4mo-based materials (previous work),[10,11] in the present case, the MCL affects only the emission intensity. In

conclusion, these results not only reveal a new series of solid-state luminescent materials, but expand the class of MCL materials, with potential applications as chemical sensors or for memory devices.

Experimental Section

Synthesis and Characterization: The bp4mo ligand has been synthesized as (bp4mo)·2H_2O according to the literature (details in the Supporting Information). As for the known [$PbCl_2$(bp4mo)] compound (**1**),[7] all the three compounds [PbX_2(bp4mo)], X = Br (**2**), X = I (**3**) and X = NO_3 (**4**) were obtained at room temperature by a slow liquid–gas diffusion method from a mixture of PbX_2 and (bp4mo)·2H_2O, which were solubilized in a minimum of DMSO [**2**: 20 mg = 5.4×10^{-5} mol $PbBr_2$ and 22 mg = 1.1×10^{-4} mol (bp4mo)·2H_2O; **3**: 64.5 mg = 1.4×10^{-4} mol PbI_2 and 26.5 mg = 1.4×10^{-4} mol (bp4mo)·2H_2O] or water [**4**: 42.2 mg = 1.3×10^{-4} mol $Pb(NO_3)_2$ and 26.5 mg = 1.4×10^{-4} mol (bp4mo)·2H_2O] with ethyl acetate (**2**, **3**) or acetone (**4**) as the counter solvent. After a few days, pale yellow crystals of **2**, yellow crystals of **3** and pale yellow crystals of **4** were obtained. All samples were filtered off and washed with ethyl acetate (**2**, **3**) or acetone (**4**) and dried in an oven at 50 °C. The comparison of the theoretical X-ray powder diffraction patterns calculated from the results of single-crystal studies and the XRPD patterns of samples [using a D8 Bruker diffractometer (Cu-$K_{\alpha 1,2}$ radiation) equipped with a linear Vantec super speed detector] clearly showed a perfect fit between the calculated and experimental lines, indicating that compounds were obtained as pure phases (Supporting Information, Figures S17–S20). TGA experiments showed that all compounds **2**–**4** are stable up to 200 °C, with decomposition occurring over 250 °C (**2**), 200 °C (**3**) and 275 °C (**4**) (Figures S21–S23). Differential scanning calorimetry was performed with a DSC-2010 TA Instruments system in the range of 20–300 °C. The grinding of the samples, which were initially put in an agate mortar, were carried out by hand. Typically, the extinction of the luminescence occurred after a few minutes grinding. The reversibility of the process was achieved by heating or fuming. This last process consisted of the exposure of the ground sample to a saturated atmosphere of solvent. Thus, the powdered sample was put into a pillbox that was inserted into a bigger pillbox containing the solvent (water or acetone). After a few hours, the solid was removed and was analyzed. The ground samples were also recrystallized by using a solution process: a few drops of acetone were added to the ground sample in such a way that all the powder was covered by the solution. After a few minutes, the solvent was fully evaporated and the solid was analyzed.

Table 1. Crystallographic data for [PbX_2(bp4mo)], X = Br (**2**), X = I (**3**) and X = NO_3 (**4**).

	2	**3**	**4**
Crystal system	monoclinic	monoclinic	orthorhombic
Space group	*C*2	*C*2/*c*	Pbca
a (Å)	16.761(1)	40.213(6)	7.664(1)
b (Å)	4.2640(4)	4.458(1)	18.293(1)
c (Å)	18.156(1)	16.935(3)	19.341(3)
β (°)	92.60(1)	110.23(1)	90
Volume (Å^3)	1296.3(2)	2848.6(9)	2711.5(6)
Z	4	8	8
Crystal density	2.763	2.953	2.466
Temperature (K)	293	293	293
Refl. collected/unique	6364/3063	21749/2988	22670/4499
Obsd. refl. [$I > 2\sigma(I)$]	2486 [0.058]	1873 [0.121]	2855 [0.066]
[R_{int}] parameters	147	147	199
$R_1[I > 2\sigma(I)]$/	0.0555/	0.0515/	0.0470/
wR_2(all data)	0.1558	0.1347	0.1380

X-ray Crystallography: X-ray diffraction data were collected at room temperature (r.t.) with a Bruker-Nonius KAPPA-CDD with Mo-K_α radiation (λ = 0.71073 Å) for all three phases. A summary of the crystallographic data and refinement results is listed in Table 1. The structures were solved by direct methods and refined on F^2 by the full-matrix least-squares method with anisotropic approximation for all non-hydrogen atoms, using the package SHELX-97.[23] All hydrogen atoms were located by the HFix routine of SHELX and absorption was corrected by the program SADABS.[24] A complete list of the crystallographic data, along with the atomic coordinates, the anisotropic displacement parameters and bond lengths and angles for each compound, are given as CIF files.

CCDC 1503146 (for **2**), 1503148 (for **3**) and 1503149 (for **4**) contain the supplementary crystallographic data for this paper. These data can be obtained free of charge from The Cambridge Crystallographic Data Centre.

Optical Absorption and Photoluminescence: UV/Vis absorption spectra were obtained with a Perkin–Elmer Lambda 900 spectrometer. PL spectra were obtained with a SPEX 270M monochromator equipped with a N_2 cooled charge-coupled device excited with a monochromated 450 W Xe lamp. The spectra were corrected for the instrument response. PL QYs were measured with a homemade integrating sphere according to the procedure reported elsewhere.[25] The photoluminescence spectra during grinding and recrystallization were measured by using a Photon Technology International LPS 220 spectrofluorometer. Time-resolved PL measurements were excited at 355 nm with the III harmonic of a Nd:YAG laser (Laser-Export Co. LCS-DTL-374QT) and detected in photon-counting mode with a Hamamatsu R943–02 photomultiplier connected to an Ortec 9353 multichannel scaler. The system was operated with an overall time resolution better than 25 ns.

Supporting Information (see footnote on the first page of this article): Synthetic procedures, single-crystal data, XRPD patterns, DSC curves, PL spectra.

Acknowledgments

O. T. and N. M. are grateful to the Pays de la Loire regional program LUMOMAT (project BipyLum) for funding and thank Bohdan Kulyk from MOLTECH-Anjou lab for second-harmonic-generation (SHG) experiments.

Keywords: Lead · N,O ligands · Coordination polymers · Luminescence · Solid-state structures

[1] a) Y. Cui, Y. Yue, G. Qian, B. Chen, *Chem. Rev.* **2012**, *112*, 1126–1162; b) J. Heine, K. Muller-Buschbaum, *Chem. Soc. Rev.* **2013**, *42*, 9232–9242; c) H. Xu, J. Wang, Y. Wei, G. Xie, Q. Xue, Z. Denga, W. Huang, *J. Mater. Chem. C* **2015**, *3*, 1893–1903; d) E. Cariati, E. Lucenti, C. Botta, U. Giovanella, D. Marinotto, S. Righetto, *Coord. Chem. Rev.* **2016**, *306*, 566–614.
[2] Y. Sagara, T. Kato, *Nat. Chem.* **2009**, *1*, 605–610.
[3] Z. Chi, X. Zhang, B. Xi, X. Zhou, C. Ma, Y. Zhang, S. Liu, J. Xu, *Chem. Soc. Rev.* **2012**, *41*, 3878–3896.
[4] X. Zhang, Z. Chi, Y. Zhang, S. Liu, J. Xu, *J. Mater. Chem. C* **2013**, *1*, 3376–3390.
[5] a) A.-C. Chamayou, C. Janiak, *Inorg. Chim. Acta* **2010**, *363*, 2193–2200; b) J. Jia, A. J. Blake, N. R. Champness, P. Hubberstey, C. Wilson, M. Schröder, *Inorg. Chem.* **2008**, *47*, 8652–8664; c) R. J. Hill, D.-L. Long, N. R. Champness, P. Hubberstey, M. Schröder, *Acc. Chem. Res.* **2005**, *38*, 335–348.

[6] D. J. Hoffart, N. C. Habermehl, S. J. Loeb, *Dalton Trans.* **2007**, 2870–2875.
[7] O. Toma, N. Mercier, M. Bouilland, M. Allain, *CrystEngComm* **2012**, *14*, 7844–7847.
[8] a) O. Toma, N. Mercier, C. Botta, *Eur. J. Inorg. Chem.* **2013**, 1113–1117; b) O. Toma, N. Mercier, M. Allain, C. Botta, *CrystEngComm* **2013**, *15*, 8565–8571.
[9] O. Toma, N. Mercier, M. Allain, A. Forni, F. Meinardi, C. Botta, *Dalton Trans.* **2015**, *44*, 14589–14593.
[10] O. Toma, N. Mercier, C. Botta, *J. Mater. Chem. C* **2016**, *4*, 5940–5944.
[11] O. Toma, M. Allain, F. Meinardi, A. Forni, C. Botta, N. Mercier, *Angew. Chem. Int. Ed.* **2016**, *55*, 7998–8002.
[12] a) J. W. Y. Lam, B. Z. Tang, *Chem. Soc. Rev.* **2011**, *40*, 5361–5388; b) J. Mei, N. L. C. Leung, R. T. K. Kwok, J. W. Y. Lam, B. Z. Tang, *Chem. Rev.* **2015**, *115*, 11718–11940.
[13] E. Quartapelle Procopio, M. Mauro, M. Panigati, D. Donghi, P. Mercandelli, A. Sironi, G. D'Alfonso, L. De Cola, *J. Am. Chem. Soc.* **2010**, *132*, 14397–14399.
[14] G. Li, Y. Wu, G. Shan, W. Che, D. Zhu, B. Song, L. Yan, Z. Su, M. R. Bryce, *Chem. Commun.* **2014**, *50*, 6977–6980.
[15] a) Z. Ma, Z. Wang, M. Teng, Z. Xu, X. Jia, *ChemPhysChem* **2015**, *16*, 1811–1828; b) C. Botta, S. Benedini, L. Carlucci, A. Forni, D. Marinotto, A. Nitti, D. Pasini, S. Righetto, E. Cariati, *J. Mater. Chem. C* **2016**, *4*, 2979–2989.
[16] a) Y. Sagara, T. Mutai, I. Yoshikawa, K. Araki, *J. Am. Chem. Soc.* **2007**, *129*, 1520–1521; b) Y. Sagara, T. Komatsu, T. Ueno, K. Hanaoka, T. Kato, T. Nagano, *Adv. Funct. Mater.* **2013**, *23*, 5277–5284; c) Y. Dong, B. Xu, J. Zhang, X. Tan, L. Wang, J. Chen, H. Lv, S. Wen, B. Li, L. Ye, B. Zou, W. Tian, *Angew. Chem. Int. Ed.* **2012**, *51*, 10782; *Angew. Chem.* **2012**, *124*, 10940–10785; d) L. Bu, M. Sun, D. Zhang, W. Liu, Y. Wang, M. Zheng, S. Xue, W. Yang, *J. Mater. Chem. C* **2013**, *1*, 2028–2035.
[17] X.-P. Zhang, J.-F. Mei, J.-C. Lai, C.-H. Li, X.-Z. You, *J. Mater. Chem. C* **2015**, *3*, 2350–2357; b) T. Abe, T. Itakura, N. Ikeda, K. Shinozaki, *Dalton Trans.* **2009**, 711–715.
[18] H. Sun, S. Liu, W. Lin, K. Y. Zhang, W. Lv, X. Huang, F. Huo, H. Yang, G. Jenkins, Q. Zhao, W. Huang, *Nat. Commun.* **2014**, *5*, 3601–3609; b) Y. Han, H.-T. Cao, H.-Z. Sun, Y. Wu, G.-G. Shan, Z.-M. Su, X.-G. Hou, Y. Liao, *J. Mater. Chem. C* **2014**, *7*, 7648–7655.
[19] P. Baranyai, G. Marsi, C. Jobbagy, A. Domjan, L. Olah, A. Deak, *Dalton Trans.* **2015**, *44*, 13455–13459.
[20] S. Perruchas, X. F. Le Goff, S. Maron, I. Maurin, F. Guillen, A. Garcia, T. Gacoin, J. P. Boilot, *J. Am. Chem. Soc.* **2010**, *132*, 10967–10969.
[21] a) H. A. Habib, A. Hoffmann, H. A. Höppe, G. Steinfeld, C. Janiak, *Inorg. Chem.* **2009**, *48*, 2166–2180; b) F. Neve, A. Crispini, *Cryst. Growth Des.* **2001**, *1*, 387–393; c) W. Zhang, X. Tang, H. Ma, W.-H. Sun, C. Janiak, *Eur. J. Inorg. Chem.* **2008**, 2830–2836.
[22] C. Janiak, *J. Chem. Soc., Dalton Trans.* **2000**, 2885–3896.
[23] G. M. Sheldrick, *SHELX-97*, *Programs for Crystal Structure Solution*, University of Göttingen, Germany, **1997**.
[24] G. M. Sheldrick, *SADABS v.2.01, Bruker/Siemens Area Detector Absorption Correction Program*, Bruker AXS, Madison, WI, USA, **1998**.
[25] J. Moreau, U. Giovanella, J.-P. Bombenger, W. Porzio, V. Vohra, L. Spadacini, G. Di Silvestro, L. Barba, G. Arrighetti, S. Destri, M. Pasini, M. Saba, F. Quochi, A. Mura, G. Bongiovanni, M. Fiorini, M. Uslenghi, C. Botta, *ChemPhysChem* **2009**, *10*, 647–653.

Received: October 6, 2016